Journal of Solid State Chemistry 204 (2013) 9–15

Contents lists available at SciVerse ScienceDirect

Journal of Solid State Chemistry

journal homepage: www.elsevier.com/locate/jssc

Cobalt-doped $Bi_{26}Mo_{10}O_{69}$: Crystal structure and conductivity

Z.A. Mikhailovskaya [a,*], E.S. Buyanova [a], S.A. Petrova [b], M.V. Morozova [a], V.M. Zhukovskiy [a], R.G. Zakharov [b], N.V. Tarakina [c,d], I.F. Berger [c]

[a] Ural Federal University, Lenin Ave. 51, 620000 Ekaterinburg, Russia
[b] Institute of Metallurgy, Ural Branch of the Russian Academy of Sciences, 101 Amundsen Str., 620016 Ekaterinburg, Russia
[c] Institute of Solid State Chemistry, Ural Branch of the Russian Academy of Sciences, 91 Pervomayskaya Str., 620990 Ekaterinburg, Russia
[d] Experimentelle Physik III, Physikalisches Institut and Wilhelm Conrad Röntgen—Research Centre for Complex Material Systems, Universität Würzburg, Am Hubland, D-97074 Würzburg, Germany

ARTICLE INFO

Article history:
Received 2 March 2013
Received in revised form
7 May 2013
Accepted 9 May 2013
Available online 20 May 2013

Keywords:
Bismuth molybdates
Oxygen-ion conductors
Crystal structure
Electrical conductivity
Impedance spectroscopy

ABSTRACT

A series of cobalt-doped bismuth molybdates were synthesized and investigated using X-ray powder diffraction, transmission electron microscopy and impedance spectroscopy. The ranges of solid solution were determined. Two new compounds, $Bi_{1-x}Co_x[Bi_{12}O_{14}]Mo_5O_{34.5\pm\delta}$ ($x=0.2$) and $Bi[Bi_{12}O_{14}]Mo_{5-y}Co_yO_{34.5\pm\delta}$ ($y=0.2$), which crystallise in monoclinic unit cells have been examined in detail by diffraction methods. Impedance spectroscopy measurements show that the studied materials are good ionic conductors with conductivity values about 5×10^{-3} S × cm^{-1} at 973 K and 1.7×10^{-4} S × cm^{-1} at 623 K, which are similar to conductivity values of yttrium substituted zirconia and (YSZ) gadolinium doped ceria (CGO).

1. Introduction

The unique properties of the Bi^{+3} ion (high polarisability, ability to form both symmetric and very asymmetric coordinations, electrochemical activity) give rise to a variety of structures and features of bismuth-based materials. Bi_2O_3–MoO_3 is one of the most widely studied bismuth oxide systems [1–5] due to the exclusive selective catalytic properties of bismuth molybdenum oxides [6–9]. The basic bismuth molybdate Bi_2MoO_6 has three polymorphic modifications [10]. The low temperature form ($L(\gamma)$-Bi_2MoO_6) is a layered Aurivillius-type phase built of alternating $(Bi_2O_2)_\infty$ and $(MoO_4)_\infty$ layers, where the latter are composed of MoO_6 distorted octahedra [11]. At 843 K $L(\gamma)$-Bi_2MoO_6 transforms reversibly into the intermediate Aurivillius-type phase I(γ'')-Bi_2MoO_6 with Mo–O layers consisting of MoO_4 tetrahedra [12]. An irreversible phase transition from the I(γ'')-phase to the H(γ')-phase takes place at 877 K. The high temperature H(γ')-Bi_2MoO_6 form has a fluorite-related network of cations with infinite channels of Bi–O polyhedra surrounded by MoO_4 tetrahedra [13,14].

Bi-rich members of the Bi_2O_3–MoO_3 system are less studied compared to the Bi_2MoO_6-based compounds. The most interesting compound in this part of the phase diagram is $Bi_{26}Mo_{10}O_{69-\delta}$ [15,16], which is isostructural to $Bi(Bi_{12}O_{14})Mo_4VO_{20}$ [17]. It consists of infinite $(Bi_{12}O_{14})_n^{8n+}$ columns, surrounded by $(Mo,V)O_4$ tetrahedra and isolated Bi atoms. Substitution of Mo and Bi by metals (Ca, Sr, Ba, Pb, W, V, etc.) was studied in several works [17,18]. $Bi_{26}Mo_{10}O_{69-\delta}$ and solid solutions are promising one-dimensional oxygen ion electrolytes and the substitution leads to a significant change of conductive properties both for better and for worse in comparison with the values of the electroconductivity of the parent compound.

The present work is devoted to the synthesis and the structural characterization of cobalt-substituted bismuth molybdates, and to establishing the relation between structural features and electrconductive properties of the obtained compounds. Substitution of bismuth and molybdenum is made possible by the closeness of the ionic radii of Co, Bi, and Mo in different coordinations: $r_{Bi}=1.17$ Å, $r_{Co}=0.9$ Å when the coordination number (c.n.) is equal to 8, and $r_{Co}=0.58$ Å, $r_{Mo}=0.41$ Å when c.n.=4 [19].

2. Material and methods

In the present work the $Bi_{1-x}Co_x[Bi_{12}O_{14}]Mo_5O_{20\pm\delta}$ ($x=0.1$–1, $\Delta x=0.1$) and $Bi[Bi_{12}O_{14}]Mo_{5-y}Co_yO_{20\pm\delta}$ ($y=0.2$, 0.4) complex oxides were synthesized. Polycrystalline samples were prepared by solid-state reaction with Bi_2O_3(99.9%), MoO_3 (99.5%) and Co_3O_4

* Correspondence to: Department of Chemistry, Ural Federal University named after the first President of Russia B.N. Yeltsin, 51 Lenin Ave., 620000, Ekaterinburg, Russia. Fax: +7 343 2617411.
E-mail address: zozoikina@mail.ru (Z.A. Mikhailovskaya).

0022-4596/$ - see front matter © 2013 Elsevier Inc. All rights reserved.
http://dx.doi.org/10.1016/j.jssc.2013.05.006

(97.5%) taken as starting compounds. Stoichiometric mixtures of initial oxides were thoroughly ground in an agate mortar, placed in alumina crucibles and annealed at temperatures in the range $T=673$–1123 K. The annealing temperature was increased step-by-step every 10 h with intermediate cooling and regrinding of the powders at each step. The phase composition of the obtained powders was monitored by X-ray powder diffraction (Bruker D8 ADVANCE, Cu$K\alpha$, VÅNTEC1, Ni-filter). The crystal structures of the compounds $Bi_{0.8}Co_{0.2}[Bi_{12}O_{14}]Mo_5O_{20\pm\delta}$ and $Bi[Bi_{12}O_{14}]Mo_{4.8}Co_{0.2}O_{20\pm\delta}$ were refined using the Rietveld method [20] in the TOPAS (Bruker) software packages [21,22] with $PbBi_{12}Mo_5O_{34}$ and $Bi_{13}Mo_5O_{34.5\pm\delta}$ [15,23] as starting models, respectively. Neutron powder diffraction patterns were collected on the D7A diffractometer ($\lambda=1.5277$ Å) at IVV-2M (Zarechnyi, Russia) in the 2θ range 1.30°–126.00° with a step of 0.05° and used to refine the positions of the oxygen atoms.

The grain size of the powders was estimated by a nanoparticle size analyzer (Shimadzu SALD-7101). Differential thermal analysis was performed on a STA 409 PC Luxx Netzsch thermoanalyzer in the temperature range 290–1070 K with alumina as a standard. The conductivity measurements were carried out in the temperature range 1070–470 K using Elins Z-2000 and Elins Z-3000 impedance spectrometers. For this purpose the powders were pressed into pellets, annealed at 1190 K during 24 h and covered with platinum. The morphology of the obtained powders and their chemical composition were studied using a Gemini Zeiss scanning electron microscope (SEM) equipped with a X-max 50 mm^2 SDD energy dispersive X-ray (EDX) detector. Chemical analysis of the samples was realized by atomic emission spectral analysis of dissolved powders of bismuth molybdates at ICAP 6500 (Thermo Sci).

The transmission electron microscopy (TEM) study was performed using a FEI (S)TEM Titan 80–300 microscope, operated at 300 kV. For the TEM study an ethanol suspension of the $Bi_{12.8}Co_{0.2}Mo_5O_{34\pm\delta}$ sample was prepared and kept in an ultrasonic bath for 5 min and then a drop of this suspension was put onto a holey carbon film supported on a Cu grid.

3. Results and discussion

3.1. Structure

At $x\leq0.2$ the $Bi_{1-x}Co_x[Bi_{12}O_{14}][MoO_4]_5$ solid solution based on the $Bi_{13}Mo_5O_{34.5\pm\delta}$ structure type, in the following referred to as B13, is observed. At $0.2<x<1$ a mixture of the B13 phase and a solid solution based on the orthorhombic $L(\gamma)$-Bi_2MoO_6 modification (Sp. gr. *Pca*21, $a=5.5019(2)$ Å, $b=16.2449(7)$ Å, $c=5.5237(1)$ Å) is formed. At $x=1$, a homogeneous powder of $Co[Bi_{12}O_{14}][MoO_4]_5$ oxide is obtained. It is isostructural to the $Bi_2Mo_{5/6}Co_{1/6}O_{6-\delta}$ bismuth molybdate, and therefore belongs to the family of $L(\gamma)$-Bi_2MoO_6 related compounds. Table 1 shows the change of the unit cell parameters of $Bi_{1-x}Co_x[Bi_{12}O_{14}][MoO_4]_5$, $x\leq0.2$ with increasing x. A smooth change of the a, c and β parameters continues up to $x=0.2$, the b parameter does practically not change because of the inflexibility of the $(Bi_{12}O_{14})_n^{8n+}$ structure elements arranged along the y axis.

The ratios of the metal elements obtained from EDX measurements of 20 grains of the $Bi_{12.8}Co_{0.2}Mo_5O_{34\pm\delta}$ sample were found to be $Bi_{12.52(07)}Co_{0.19(01)}Mo_{5.00(04)}$ which is in a good agreement with the nominal composition and the chemical analysis data (Table 1 in the Supplementary Material). The variations in the cobalt content from grain to grain can be attributed to both the usually much higher error of EDX analysis for low concentrations of elements and to the inhomogeneous distribution of Co in the sample.

The $Bi[Bi_{12}O_{14}]Mo_{5-y}Co_yO_{20\pm\delta}$ solid solution exists up to $y=0.2$. Increasing the dopant concentration leads to the formation of the H(γ')-Bi_2MoO_6 phase and a $Bi_{38}Mo_7O_{78}$-based solid solution or mixtures of different bismuth molybdates.

The compositions $Bi_{12.8}Co_{0.2}Mo_5O_{34\pm\delta}$ and $Bi_{13}Mo_{4.8}Co_{0.2}O_{34\pm\delta}$ from each solid solution were selected for a detailed crystal structure study.

XRPD pattern obtained with high resolution data collection were used for refining structures. At the $Bi_{12.8}Co_{0.2}Mo_5O_{34\pm\delta}$ XRPD pattern a small amount (~0.1%) of H(γ')-Bi_2MoO_6 (monocl) was detected. Related to this impurity parts of the XRPD spectrum were excluded from the calculation. Presence H(γ')-Bi_2MoO_6 was not observed by the electron microscopy, but it can explain small deviation of composition of $Bi_{12.8}Co_{0.2}Mo_5O_{34\pm\delta}$ from the theoretical formula, as was detected by EDX-analysis indicated above. An analysis of systematically absent reflections in the XRPD pattern of $Bi_{12.8}Co_{0.2}Mo_5O_{34\pm\delta}$ indicates a $P2/c$ space group. $PbBi_{12}Mo_5O_{34}$ was used as a starting model for the crystal structure refinement. The details of the refinement, refined atomic coordinates and temperature factors for $Bi_{12.8}Co_{0.2}Mo_5O_{34\pm\delta}$ are given in Tables 2 and 3 and Fig. 1. The final structure is represented in Fig. 2. A decrease of the a, c and β unit cell parameters in comparison with the parent is observed. The same tendency also occurs in some other bismuth molybdates with the B13 crystal structure type, for example $PbBi_{12}Mo_5O_{34}$ [23]. This phenomenon can be explained either by the smaller radius of cobalt or by the absence of the ns^2 isolated electron pair in the cobalt atom.

Selected area electron diffraction (SAED) patterns were indexed in a monoclinic unit cell with parameters: $a\approx$ 11.9 Å, $b\approx$5.84 Å, $c\approx$24.8 Å, $\beta\approx$102.3°, which is in agreement with the XRPD data. The analysis of the extinction conditions ($h\,0\,l$: $l=2n$; $0\,0\,l$: $l=2n$) point towards two possible space groups: Pn (7) and $P2/n$ (13). The appearance of the forbidden reflections $0\,0\,l$ ($l=2n$) on the [1 0 0]* pattern is due to double diffraction; this is seen by the fact that the reflections disappear when rotating the crystal away from the perfect orientation around this axis (Fig. 3). Weak lines of diffuse scattering along the $\boldsymbol{c}^*$ direction observed in most of the SAED patterns indicate the presence of disorder in this compound.

A high-resolution transmission electron microscopy (HRTEM) image of $Bi_{12.8}Co_{0.2}Mo_5O_{34\pm\delta}$ obtained along the [0 1 0] axis is shown in Fig. 4, the intense white reflections correspond to the voids in the structure; this is confirmed by the simulated image.

Table 1
Dependence of the unit cell parameter of $Bi_{1-x}Co_x[Bi_{12}O_{14}][MoO_4]_5$ on x.

Compound $Bi_{1-x}Co_x[Bi_{12}O_{14}][MoO_4]_5$	Unit cell parameters			
	a, Å	b, Å	c, Å	β, °
$Bi[Bi_{12}O_{14}][MoO_4]_5$	11.790	5.801	24.706	102.8
$Bi_{0.9}Co_{0.1}[Bi_{12}O_{14}][MoO_4]_5$	11.767	5.801	24.698	102.5
$Bi_{0.8}Co_{0.2}[Bi_{12}O_{14}][MoO_4]_5$	11.723	5.796	24.699	102.1

Table 2
Crystal data for $Bi_{12.8}Co_{0.2}Mo_5O_{34\pm\delta}$ and $Bi_{13}Mo_{4.8}Co_{0.2}O_{34\pm\delta}$.

	$Bi_{12.8}Co_{0.2}Mo_5O_{34\pm\delta}$
Space group	$P2/c$
Unit cell parameters	$a=11.7226(6)$ Å $b=5.7959(2)$ Å $c=24.6994(11)$ Å $\beta=102,.08(1)°$
Unit cell volume (Å^3)	1640.92(2)
Formula units, Z	2

Table 3
Fractional atomic coordinates and isotropic temperature factors for $Bi_{12.8}Co_{0.2}Mo_5O_{34\pm\delta}$.

Atom	Site	x	y	z	Occupancy	Biso
Bi1	4g	0.0410(2)	0.4116(4)	0.3270(1)	0.96(2)	0.59(8)
Bi2	4g	0.1614(2)	–0.0873(4)	0.2450(1)	0.99(2)	0.73(8)
Bi3	4g	0.2424(2)	0.0043(5)	0.4003(1)	0.99(2)	0.75(7)
Bi4	4g	0.3599(2)	0.4955(5)	0.3225(1)	0.98(2)	0.81(7)
Bi5	4g	0.2718(2)	0.4941(6)	0.1587(1)	0.99(2)	0.82(7)
Bi6	4g	0.0811(2)	0.0010(5)	0.0913(1)	1.00(2)	0.75(7)
Bi7/Co	4g	0.5173(8)	0.4655(1)	0.0112(3)	0.38/0.12(1)	0.95(8)
Mo1	2f	0.5	0.0130(16)	0.25	0.95(3)	0.94(7)
Mo2	4g	0.1645(4)	0.5104(10)	0.4887(2)	0.96(2)	1.11(16)
Mo3	4g	0.4239(4)	0.0004(10)	0.0777(2)	0.96(2)	1.02(16)
O1*	2f	0	0.246(8)	0.25	0.79(4)	0.30(9)
O2*	2f	0	–0.256(7)	0.25	0.72(4)	0.30(9)
O3*	4g	0.245(2)	0.256(3)	0.339(1)	0.99(4)	0.71(11)
O4*	4g	0.227(2)	0.753(3)	0.335(1)	0.84(4)	0.25(7)
O5*	4g	0.267(2)	0.591(3)	0.242(1)	0.73(3)	0.59(10)
O6*	4g	0.134(2)	0.757(4)	0.146(1)	0.93(4)	0.98(14)
O7*	4g	0.138(2)	0.236(3)	0.150(1)	0.97(4)	1.07(17)
O8*	4g	0.069(2)	0.041(3)	0.361(1)	0.97(3)	1.44(22)
O9*	4g	0.426(4)	0.240(7)	0.230(2)	0.30(2)	0.84(21)
O10*	4g	0.378(2)	0.171(4)	0.241(1)	0.71(2)	0.84(21)
O11*	4g	0.510(3)	–0.066(7)	0.174(2)	0.43(2)	0.98(13)
O12*	4g	0.466(2)	–0.173(3)	0.179(1)	0.73(2)	0.98(13)
O13*	4g	0.400(2)	0.100(3)	0.010(1)	0.99(3)	1.33(27)
O14*	4g	0.294(2)	–0.014(4)	0.101(1)	0.96(4)	1.25(21)
O15*	4g	0.470(2)	–0.272(3)	0.074(1)	0.99(4)	1.01(15)
O16*	4g	0.541(2)	0.189(4)	0.094(1)	0.79(4)	0.88(12)
O17*	4g	0.255(1)	0.581(3)	0.550(1)	0.92(3)	1.24(23)
O18*	4g	0.287(1)	0.420(3)	0.455(1)	1.00(3)	0.98(12)
O19*	4g	0.107(25)	0.766(3)	0.464(1)	1.00(3)	1.29(21)
O20*	4g	0.080(2)	0.265(3)	0.485(1)	1.00(3)	0.91(19)

R_B=1.901 (6.158)*, R_{exp}=1.90 (1.65)*, R_{wp}=4.01 (4.32)*, R_p=2.96 (3.28)*, χ^2=2.12 (2.62)*.

* Neutron powder diffraction data.

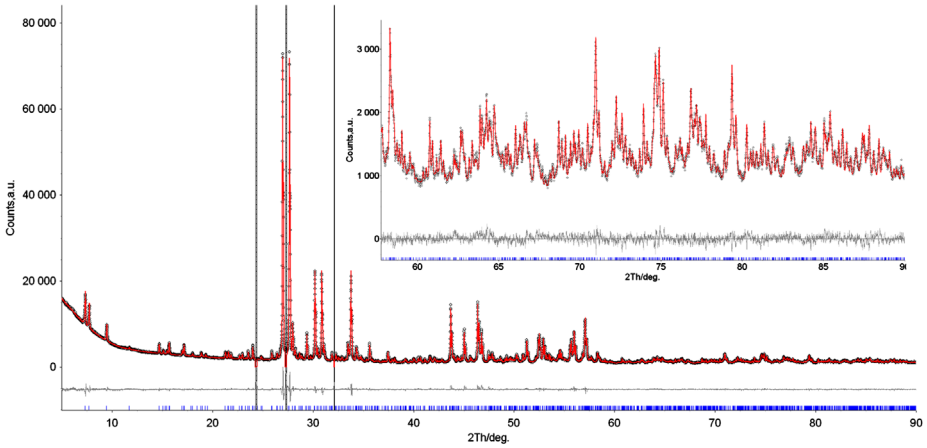

Fig. 1. Measured and calculated diffraction XRPD pattern, the difference curve, and line diagram for a $Bi_{12.8}Co_{0.2}Mo_5O_{34\pm\delta}$ sample calculated on the assumption of monoclinic space group *P*2/*c*. In inset, fragment of the XRPD pattern with magnification along axis *y*.

Neutron powder diffraction data were used to refine the positions of the oxygen atoms. Significant changes in molybdenum–oxygen polyhedra were observed. In contrast to the structure of the parent compound Bi13 which consists of symmetric regular tetrahedra, the structure of the cobalt-doped molybdate consists of distorted octahedra and tetrahedra. Distortions of the Mo–O polyhedra are not equivalent for different molybdenum positions. The coordination of the Mo3 atoms is fixed because of the close contact with the $[Bi_{12}O_{14}]_n^{8n+}$ columns. In contrast, Mo1 and Mo2 form oxygen polyhedra which are weakly connected with $[Bi_{12}O_{14}]_n^{8n+}$ columns, and thereby the positions of these oxygen (O10, O11, O12, O17, O18, O19, O20) atoms are more variable. This allows the formation of different coordination polyhedra around Mo1 and Mo2 atoms: tetrahedral, distorted octahedral and asymmetric triangular pyramidal (which can be described as an octahedron with one epical and one axial oxygen vacancy). As a result such structural flexibility is responsible for the increase of the quantity of structural oxygen vacancies (or vacant interstitial site of oxygen) or increase of oxygen vacancies mobility, which improves the electrical conductivity of these compounds (Table 4).

The XRPD pattern of $Bi_{13}Mo_{4.8}Co_{0.2}O_{34\pm\delta}$ has been indexed in a monoclinic unit cell, *P*2/*c* space group, with parameters: a=11.7171(6) Å, b=5.7924 (1) Å, c=24.7405(10) Å, β=102.68(1)°, V=1631.33(02) Å^3 (R_B=2.01, R_{exp}=2.60, R_{wp}=3.53). Characteristic changes of the *a*, *c*, β values as compared with the parent compound are also observed. $Bi_{13}Mo_5O_{34.5\pm\delta}$ (B13) was used as

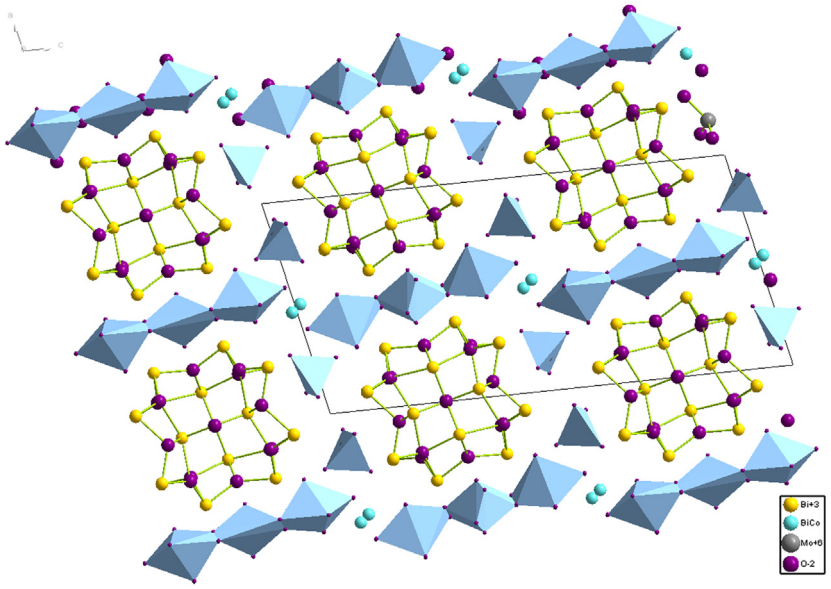

Fig. 2. Projection of the $Bi_{12.8}Co_{0.2}Mo_5O_{34\pm\delta}$ crystal structure onto the *ac* plane: grey spheres in "roses" are Bi atoms, double spheres are Bi/Co atoms, dark grey spheres are oxygen atoms, polyhedra are the MoO_4 units.

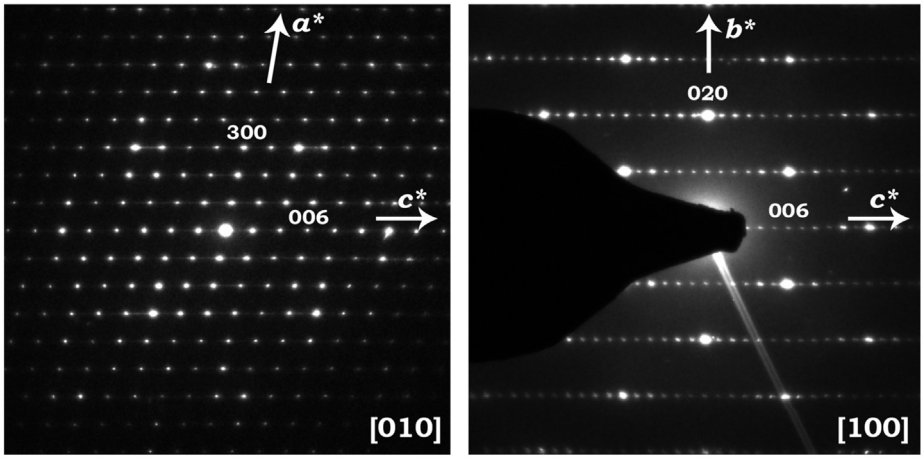

Fig. 3. Selected area electron diffraction patterns of $Bi_{12.8}Co_{0.2}Mo_5O_{34\pm\delta}$ recorded along the [0 1 0]* and [1 0 0]* axis.

a starting model for the crystal structure refinement. Details of substitution of molybdenum by cobalt are not detected in this case because of low quantity of atoms of cobalt per one atom of molybdenum (0.2 Co:4.8 Mo atoms=0.041, simultaneously cobalt substituted bismuth provides to relationship: 0.2 Co:1 Bi atom).

A comparison of the unit cell parameters with the data of Bastide et al. [24] shows similarity of the obtained values with those for Mg-doped bismuth molybdate ($Bi_{13}Mo_{4.75}Mg_{0.25}O_{34\pm\delta}$), which can be explained by the closeness of the ionic radii of Mg and Co (r_{Co}=0.58 Å, r_{Co}=0.57 Å [19]) in tetrahedral coordination. It could also be an indication of the low valence state (+2) of the cobalt atoms.

However, formal substitution of molybdenum or bismuth by cobalt is considered to be a more complex process, which can include a substitution of the isolated bismuth atoms by cobalt with subsequent replacement of molybdenum atoms by the very same bismuth atoms. This process is possible due to the formation of the distorted $[BiO_3E]$ tetrahedra in the structure of doped bismuth molybdates (E is the $6s^2$ isolated electron pair of bismuth [17,24]). In the Bi13 parent compound, where bismuth atoms have octahedral coordination, the $[BiO_3E]$ tetrahedra are absent. But in substituted bismuth molybdate polyhedron $[BiO_3E]$ can be present.

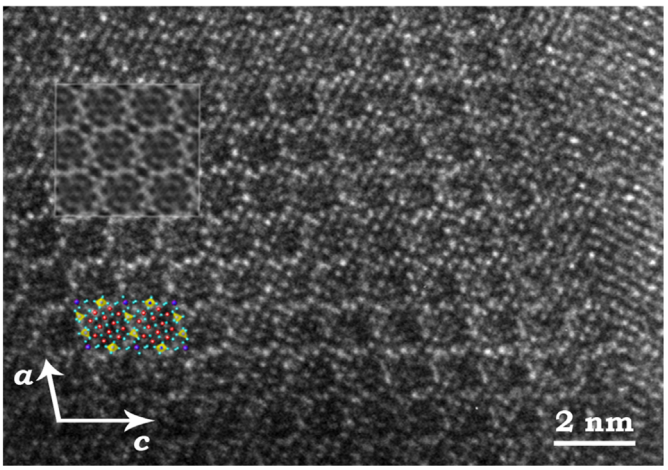

Fig. 4. [0 1 0] HRTEM image of $Bi_{12.8}Co_{0.2}Mo_5O_{34\pm\delta}$. The simulation for a defocus of −17 nm and a thickness of 4.7 nm was done using the crystal structure model obtained from the XRPD study; it is indicated by a white border. A model structure is shown at the lower left corner (Bi and O atoms are shown as spheres, tetrahedra correspond to the MoO4 units).

Table 4
Selected interatomic distances for $Bi_{12.8}Co_{0.2}Mo_5O_{34\pm\delta}$.

At.1		At.2	d12, Å	At.1		At.2	d12, Å	At.1		At.2	d12, Å
Bi1	–	O1	2.09	Bi4	–	O4	2.31	Bi7/Co	–	O18	2.29
Bi1	–	O8	2.31	Bi4	–	O14	2.78	Bi7/Co	–	O15	2.32
Bi1	–	O7	2.49	Bi4	–	O11	2.79	Bi7/Co	–	O15	2.42
Bi1	–	O3	2.51	Bi4	–	O12	2.51	Bi7/Co	–	O13	2.53
Bi1	–	O2	2.68	Bi5	–	O7	2.15	Bi7/Co	–	O18	2.85
Bi2	–	O2	2.16	Bi5	–	O5	2.15	Mo1	–	O10	1.60
Bi2	–	O5	2.25	Bi5	–	O6	2.19	Mo1	–	O11	1.68
Bi2	–	O4	2.39	Bi5	–	O9	2.68	Mo1	–	O12	2.03
Bi2	–	O6	2.56	Bi5	–	O10	2.69	Mo2	–	O19	1.68
Bi2	–	O1	2.72	Bi5	–	O17	2.85	Mo2	–	O17	1.70
Bi3	–	O8	2.07	Bi6	–	O6	1.97	Mo2	–	O20	1.73
Bi3	–	O4	2.15	Bi6	–	O7	2.01	Mo2	–	O18	1.87
Bi3	–	O3	2.10	Bi6	–	O8	2.31	Mo3	–	O15	1.67
Bi3	–	O19	2.73	Bi6	–	O14	2.45	Mo3	–	O16	1.74
Bi4	–	O3	2.04	Bi6	–	O19	2.70	Mo3	–	O13	1.74
Bi4	–	O5	2.12	Bi6	–	O20	2.82	Mo3	–	O12	1.74

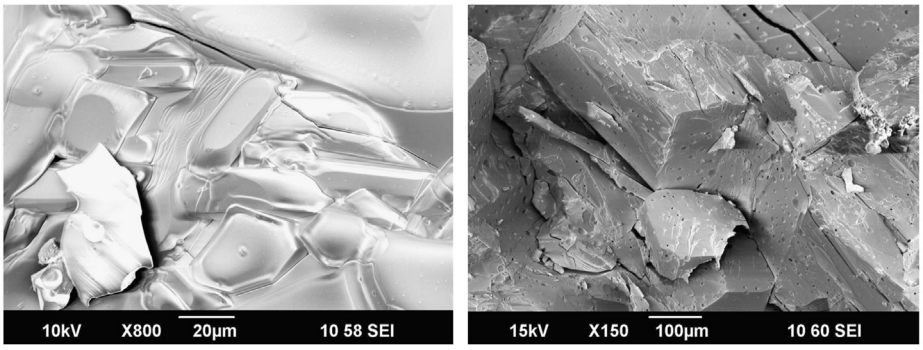

Fig. 5. SEM image of bismuth molybdates pellets split of the $Bi_{12.8}$ $Co_{0.2}Mo_5O_{34\pm\delta}$: surface and interior.

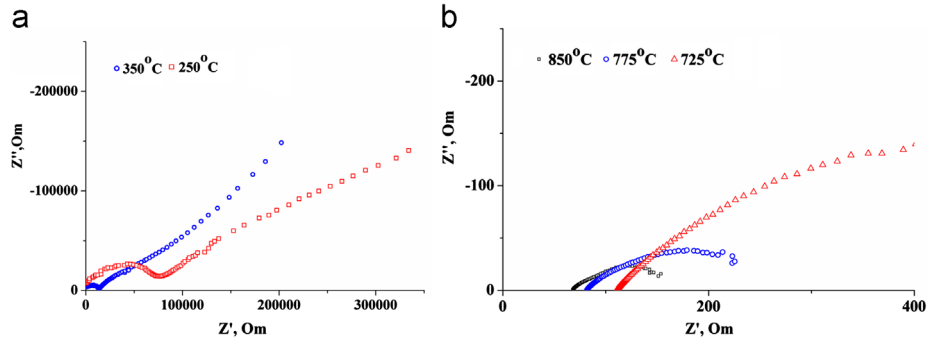

Fig. 6. The typical form of the complex plane plots for $Bi_{13}Mo_{4.8}Co_{0.2}O_{34\pm\delta}$ at low (a) and high temperatures (b).

Probably in the future this phenomenon will be confirmed by using IR spectroscopy.

3.2. Conductivity and characteristics of the ceramic samples

The synthesized complex oxides can be used as materials for electrochemical devices. The main requirements for these materials are: the formation of the bulk ceramics with low thermal expansion coefficients, absence of phase transitions and high values of the electrical conductivity in the range of operating temperatures.

Changes in sample mass and thermal effects for the $Bi_{13}Mo_{4.8}$-$Co_{0.2}O_{34-\delta}$ were studied by Differential Thermal analysis and Differential Scanning Calorimetry in the 300–1120 K temperature range. No phase effects were observed; it indicates the absence of phase transitions and decomposition processes of complex oxides in the above-mentioned temperature range in air, indicating stability a monoclinic modification. A dilatometer was used to determine the thermal expansion coefficient. The value of 14×10^{-6} K^{-1} found for mentioned compound, which is typical for ceramics. The absence of phase transitions in the sample has been also confirmed.

The particle sizes of the synthesized powders lie in the range of 1–10 μm. After the final annealing of the powders pellets were formed and annealed at 1123 K for 12 h. Scanning microscopy shows essential grain growth. Large grains (about hundreds of microns) and isolated spherical pores are seen in Fig. 5, indicating the formation of bulk ceramics.

Two pieces of pellets were coated with platinum and subjected to impedance spectroscopy in the range of 1123–523 K. Fig. 6

shows examples of complex plane plots for $Bi_{13}Mo_{4.8}Co_{0.2}O_{34-\delta}$ at different temperatures.

This shape of complex plane plots is typical for all studied compositions. Equivalent electrical circuits for the processes taking place over a certain temperature range were selected using the Zview software (Version 2.6b, Scribner Associates, Inc.).

At relatively low temperatures (300–500 °C), one can see on the complex plane plot a first semicircle turning into a fragment of a second semicircle, which turns into a line. The slope of this line is close to 45°. In the low-temperature region the circuit is a series connection of resistances *R*1, *R*2, in parallel with the associated elements CPE1, CPE2, and a shot Warburg diffusion element W1 (Fig. 7a). The CPE-like elements in the equivalent circuit are the constant phase elements. The resistance *R*1 and the element CPE1 correspond to the bulk conductivity of the sample. Parallel connection of *R*2 and CPE2 corresponds to the grain boundary conductivity and the sum of *R*1 and *R*2 corresponds to the total resistance of the sample. Thus, the conductivity of the polycrystalline sample at low temperatures was calculated according to the *R*1+*R*2 value. The Warburg element Ws describes the processes at the electrodes including diffusion and the electrochemical process on the surface. The orders of magnitude for the CPE1 and CPE2 "capacitances" are equal to 10^{-11} and 10^{-6} F, respectively. Therefore we can assign them to the grain boundary conductivity and the electrochemical process, respectively [25].

When increasing the temperature, the processes of diffusion and oxygen adsorption on the electrodes are simplified, and the Warburg diffusion element disappears from the equivalent circuit (Fig. 7b). This is why at moderate temperatures the complex plane plots look like a semicircle of smaller radius, turning into a semicircle of large radius (Fig. 6b).

At high temperatures the smaller semicircle can be described by a/the *R*2 and CPE1 connection and corresponds to the grain boundary conductivity. The semicircle of volume conductivity disappears and the volume resistance is characterized only by the value of *R*1. Thus, the sum of *R*1 and *R*2 characterize the total resistance of the sample. The "capacitance" of CPE1 is about 10^{-11} F, which is typical for oxide systems. Parallel connection of *R*3 and CPE2 describes electrochemical processes at the electrodes, which cannot be detected at low temperatures because of the domination of diffusion processes.

A significant increase of the electrical conductivity for single-phase doped compounds with respect to the matrix compound is revealed. This phenomenon is well correlated with the theoretical increase of oxygen vacancies shown by neutron diffraction studies. Concentration and temperature dependences of electrical conductivity are presented in Fig. 8a and b. It was found that substitution of molybdenum by cobalt led to higher values of electrical conductivity than the substitution of the same quantity of bismuth by cobalt. Probably, the doping at the molybdenum sublattice is more effective due to the transition of isolated bismuth atoms into the molybdenum sublattice and the formation of BiO_3E tetrahedra. For example, Bastide et al. [26] assumed that the isolated $6s^2$ electron pair of isolated bismuth atom prevents oxygen diffusion and extraction of the atom from an isolated position increases the electrical conductivity.

However, the increase of conductivity is a short-term effect, as with an increase of dopant concentration the second phase appears and a significant decrease of the electrical conductivity is observed. The values of activation energy and conductivity at various temperatures for the studied bismuth molybdates and certain materials are compared in Table 5. It is seen that in the temperature range 670–770 K these materials can rival with conventional oxygen-ion conductors. At the same time the high quality of ceramics makes the investigated materials promising as electrolytes for electrochemical devices.

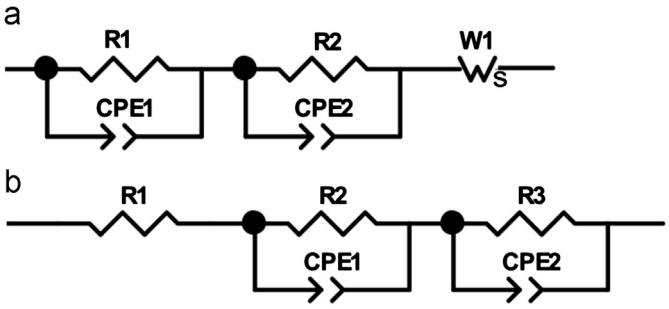

Fig. 7. Equivalent electrical circuits of electrochemical cells at: (a) low (498–823 K); and (b) high (873–1098 K) temperature regions.

4. Conclusion

In this study, we have synthesized the cobalt-substituted bismuth molybdates with general formulae $Bi_{1-x}Co_x[Bi_{12}O_{14}]$

Table 5
The values of activation energy and conductivity for bismuth molybdates and conventional oxide materials at various temperatures.

Compound	$-\lg \sigma_{700}$, S × cm^{-1}	$-\lg \sigma_{350}$, S × cm^{-1}	E_{akt}, eV
$Bi_{0.8}Co_{0.2}[Bi_{12}O_{14}]Mo_5O_{20\pm\delta}$	2.24	3.87	0.52
$Bi[Bi_{12}O_{14}]Mo_{4.8}Co_{0.2}O_{20\pm\delta}$	2.23	3.74	0.51
$Ce_{0.8}Gd_{0.2}O_{1.9}$ [27]	~1.9	~5	1.03
YSZ [28]	~1–2	~3.5–4.5	~0.9–1.05

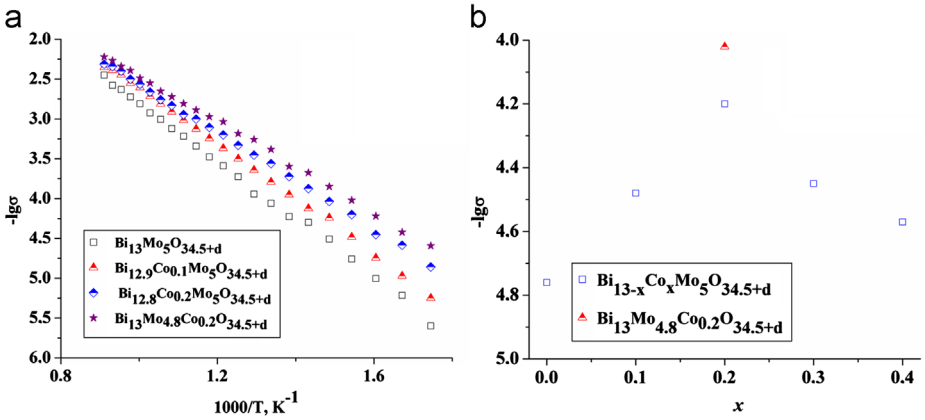

Fig. 8. Temperature (a) and concentration (b) dependences of electrical conductivity of substituted bismuth molybdates.

$Mo_5O_{20\pm\delta}$ ($x=0.1$–1, $\Delta x=0.1$) and $Bi[Bi_{12}O_{14}]Mo_{5-y}Co_yO_{20\pm\delta}$ ($y=0.2$, 0.4) by conventional solid state technology. The solid solutions exist up to $x=0.2$ and $y=0.2$ have monoclinic unit cell (Sp.gr. $P2/c$). There were revealed changes of structure of solid solutions in comparison to the structure of the parent compound such as distortions of the Mo–O polyhedra. These variations of structure lead to increase of electroconductivity values, measured by impedance spectroscopy. Total c x onductivity of bismuth molybdates are about 5×10^{-3} S × cm^{-1} at 973 K and 1.7×10^{-4} S × cm^{-1} at 623 K.

Acknowledgments

This work was financially supported by the Russian Fund of Basic Research (project No 12-03-00464 and 12-03-3119). N.V.T. acknowledges funding by the Bavarian Ministry of Sciences, Research and the Arts.

Appendix A. Supporting information

Supplementary data associated with this article can be found in the online version at http://dx.doi.org/10.1016/j.jssc.2013.05.006.

References

[1] L. Ya., E.L. Erman, Galperin, B.P. Soboler, Russ. J. Inorg. Chem. (Engl. Transl.) 16 (1971) 258–263.
[2] S. Miyazawa, A. Kawana, H. Koizumi, Mater. Res. Bull. 9 (1974) 41–51.
[3] T. Chen, S. Smith, J. Solid State Chem. 13 (1975) 288–297.
[4] D.J. Buttrey, D.A. Jeferson, J.M. Thomas, Mater. Res. Bull. 21 (1985) 739–744.
[5] L.E. Depero, L. Sangaleti, J. Solid State Chem. 119 (1995) 428–431.
[6] R.K. Grasselli, Appl. Catal., A 15 (1985) 127–139.
[7] J.D. Burrington, C.T. Kartisek, R.K. Grasselli, J. Catal. 87 (1984) 363–380.
[8] D.J. Hucknall, Selective Oxidation of Hydrocarbons, Academic Press, New York, 1974.
[9] T. Uda, T. Lin, G.W. Keulks, J. Catal. 62 (1980) 26–34.
[10] H. Kodama, A. Watanabe, J. Solid State Chem. 56 (1985) 225–229.
[11] K.S. Knight, Miner. Mag. 56 (1992) 399–409.
[12] V.I. Voronkova, E.P. Kharitonova, O.G. Rudnitskaya, J. Alloys Compd. 487 (2009) 274–279.
[13] D.J. Buttrey, T. Vogt, U. Wildgruber, W.R. Robinson, J. Solid State Chem. 111 (1994) 118–127.
[14] P. Bégué., R. Enjalbert, J. Galy, A. Castro, Solid State Sci. 2 (2000) 637–653.
[15] R.N. Vannier, G. Mairesse, F. Abraham, G. Nowogrocki, J. Solid State Chem. 122 (1996) 394–406.
[16] D.J. Buttrey, T. Vogt, G.P.A. Yap, A.L. Rheingold, Mater. Res. Bull. 32 (1997) 947–962.
[17] R. Enjalbert, G. Hassselmann, J. Galy, J. Solid State Chem. 131 (1997) 236–245.
[18] R.N. Vannier, S. Danze, G. Nowogrocki, M. Huve, G. Mairesse, Solid State Ionics 136-137 (2000) 51–59.
[19] R.D. Shannon, Acta Crystallogr., Sect. A: Found. Crystallogr. 32 (1976) 751–767.
[20] H.M. Rietveld, J. Appl. Crystallogr. 2 (1969) 65–71.
[21] Diffrac^{Plus}: Topas Bruker AXS GmbH, Ostliche. Rheinbruckenstraße 50, D-76187, Karlsruhe, Germany 2009.
[22] J. Rodriguez-Carvajal, Phys. B: Condens. Matter Quanta 192 (1993) 55–69.
[23] R. Enjalbert, G. Hasselmann, J. Galy, Acta Crystallogr., Sect. C: Cryst. Struct. Commun. 53 (1997) 269–272.
[24] B. Bastide, R. Enjalbert, P. Salles, J. Galy, Solid State Ionics 158 (2003) 351–358.
[25] J.T.S. Irvine, D.C. Sinclair, A.R. West, Adv. Mater. 2 (1990) 132–138.
[26] B. Bastide, S. Villain, R. Enjalbert, J. Galy, Solid State Sci. 4 (2002) 599–608.
[27] E.Yu. Pikalova, A.A. Murashkina, V.I. Maragou, A.K. Demina, V.N. Strekalovsky, P.E. Tsiakaras, Int. J. Hydrogen Energy 36 (2011) 6175–6183.
[28] J.H. Joo, G.M. Choi, Solid State Ionics 177 (2006) 1053–1057.